This study was undertaken to apply MDCT for 3D imaging of the trabecular microarchitecture of human vertebrae and to evaluate the use of the microstructure parameters obtained by MDCT for the assessment of fracture risk in postmenopausal women.

MATERIALS AND METHODS

Specimen study

Specimens: Five formalin-fixed specimens of vertebrae of female cadavers (62–83 years of age at the time of death) were obtained from Tokyo Metropolitan Institute of Gerontology and Geriatrics Hospital. These vertebrae were used to define the appropriate scanning milli-ampere second value within clinically available values that revealed trabecular microstructure with a low signal-to-noise ratio. To compare the MDCT images with those obtained by μCT, we mounted the excised vertebral specimens on a sample holder of 40 mm diameter filled with an 8% gelatinous solution containing 88% protein, 1% mineral, and 11% water to keep the specimens steady. Specimens that contained air on CT images were excluded. The study protocol was approved by the ethical committee of Tokyo Metropolitan Institute of Gerontology and Geriatrics.

Imaging by μCT: μCT scanning was performed ex vivo on excised human vertebrae to validate MDCT images and data. A μCT apparatus (μCT40) and its analysis software were purchased from SCANCO Medical (Basserdorf, Switzerland).[7] Details of an earlier model (μCT20) were described previously.[8] The process was piloted by an Alpha DS10 workstation (Compaq Computer Corp.), and an open VMS system in a cluster configuration was used to perform 3D analysis. Each specimen was positioned as so to permit scanning of 600 slices with 40-μm increments with a spatial resolution of ~40 μm.

Imaging by MDCT: After μCT scanning, bone specimens in the holder were placed in a 20-cm thickness water-equivalent solid phantom (Standard Grade Solid Water Gammex 457; GAMMEX RMI) and scanned by MDCT. Axial CT images with a collimation of 0.5 mm, a table feed of 2 mm, and a reconstruction index of 0.3 mm were obtained with a MDCT system having four detectors (SOMATOM plus 4 Volume Zoom; Siemens, Erlangen, Germany). An ultra-high spatial resolution kernel was applied (head, filter H 70 very sharp). CT scanning of excised vertebra was performed with the following scanning conditions: field of view (FOV) of 100 mm and pixel matrix of 512 × 512, leading to a maximal spatial resolution of ~250 × 250 × 500 μm^3.

We first determined optimal conditions for MDCT scanning by using excised human vertebrae and compared the MDCT data with those obtained by μCT as a reference. Figure 1 shows images of an excised human vertebra obtained by μCT (Fig. 1A, with the volume of interest shown by a square), high-resolution CT images obtained by MDCT at 200, 250, and 300 mAs (Fig. 1B), their binarized images (Fig. 1C), and reconstructed 3D images (Fig. 1D). Scanning at 350 mAs was not performed because of overload of X-ray tube use for clinical cases. Measurements were repeated at the same position five times, and precision of repeated measurements was 2.35 ± 0.56% for bone volume/total volume (BV/TV), 2.21 ± 2.91% for trabecular number (Tb.N), 3,17 ± 3.28% for trabecular thickness (Tb.Th), 3.62 ± 1.29% for trabecular separation (Tb.Sp), 7.45 ± 1.26% for Euler's number, 4,08 ± 1.48% for structural model index (SMI), and 4.21 ± 1.42% for fractal dimension (n = 3 each).

Structure analysis: Both MDCT image data and μCT data were transferred to a workstation (Precision 360; Dell), and structural indices were calculated using a 3D image analysis system (TRI/3D-BON; RATOC System Engineering Co., Tokyo, Japan). To compare the parameters between μCT images and MDCT images, we defined the volume of interest (VOI) in μCT images first, and then adjusted it for MDCT images with reference to the VOI in μCT images. Grayscale images were segmented by using a median filter to remove noise with a fixed threshold to extract mineralized bone components. We used a standardized method of image thresholding based on the density histogram of a selected region of interest (ROI) to ensure consistency in the image thresholding across all subjects studied. Isolated small particles in the marrow space and isolated small holes in bone were removed by using a cluster-labeling algorithm.

Trabecular microstructure parameters were calculated in 3D as follows: bone volume (BV) was calculated using tetrahedrons corresponding to the enclosed volume of the triangulated surface. Total tissue volume (TV) was the entire volume of analysis, and apparent trabecular bone volume fraction (app BV/TV) was calculated from these values. Apparent trabecular thickness (app Tb.Th) was determined according to the method described by Hildebrand and Ruggsegger.[9] Apparent trabecular number (app Tb.N) and apparent trabecular separation (app Tb.Sp) were estimated based on the plate model.[10]

In addition to the computation of metric parameters, nonmetric parameters were calculated to obtain the 3D nature of the trabecular bone samples. Fractal dimensions of trabecular bone were measured as a representative of complexity using the box-counting method[11] that was developed in 3D. Connectivity was calculated by using the Euler method of Odgaard and Gundersen (Euler's number).[12] Degree of anisotropy (DA) was determined from the ratio between the maximal and minimal radii of the mean intercept length (MIL) ellipsoid.[13]

The interactive analysis time, including data examination, ROI definition, and image segmentation, was ~10 minutes for each type of data.

Biomechanical study

Specimens and microstructure analysis: Four femoral head specimens were obtained during surgery for femoral neck fracture at Nagasaki Rosai Hospital (2 men, 70 and 78 years of age; 2 women, 83 and 85 years of age). Surrounding soft tissues were removed, and 10-mm^3 specimens were prepared and stored at –20°C before use. The study protocol was approved by the ethical committee of Nagasaki Rosai Hospital.

These specimens were placed in an acrylic tank containing physiological saline solution and scanned by MDCT. Scanning direction was adjusted to the direction of loading

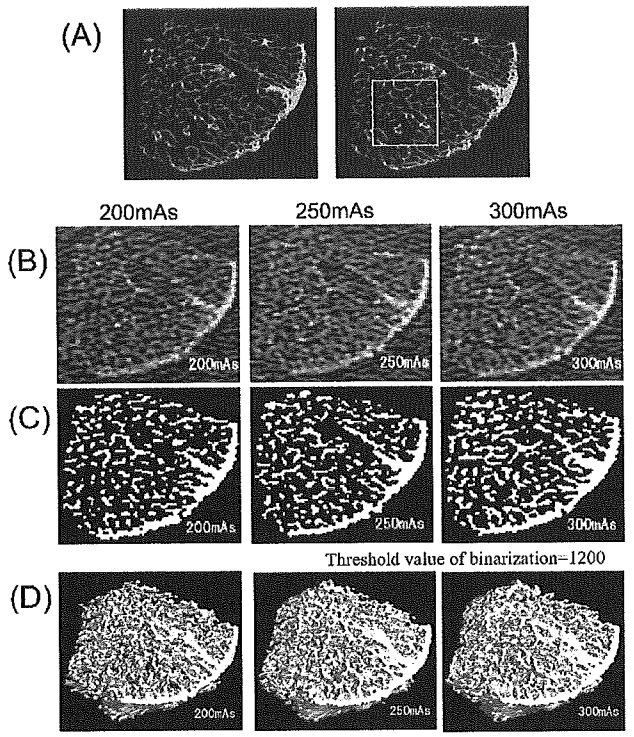

Threshold value	mAs	r	p
1120	200	0.656	ns
	250	0.487	ns
	300	0.959	< 0.01
1200	200	0.665	ns
	250	0.899	< 0.05
	300	0.979	< 0.005
1280	200	0.629	ns
	250	0.886	< 0.05
	300	0.959	< 0.05

FIG. 1. Visualization of spinal microstructure by MDCT scanning. Representative images of excised human vertebrae by (A) μCT image (volume of interest delimited by the square) and (B–D) MDCT images are shown. MDCT images were obtained under different conditions at 200, 250, and 300 mA; each CT image was analyzed at different threshold values (1120, 1200, and 1280). (B) Original 2D MDCT images at 200, 250, and 300 mA. (C) Binarized 2D CT images at 200, 250, and 300 mAs. (D) 3D CT images at 200, 250, and 300 mAs. The binarized and 3D images were prepared by using a threshold value of 1200. The linear correlations (r) and statistical significances (p) between apparent BV/TV measured by μCT and MDCT at 200, 250, and 300 mAs are also shown at the right.

in the biomechanical test. The scanning condition was the same as in the cadaver specimen study described above. Microstructure parameters were obtained for all of the specimens by the same procedure described above.

Determination of bone strength by compression test: Specimens were placed centrally on the compression testing fixture, which is able to hold the specimen stably in the cylinder and load only compressive direction without rotation or bending, and was attached to the materials-testing machine (Instron model 5582). A compression force was applied in a cranio-caudal direction using the fixture at a nominal deformation rate of 0.5 mm/minute and a sampling rate of 20 Hz. Crosshead displacement was recorded as specimen deformation. A load-deformation curve was displayed with a monitoring recorder linked to the tester in each specimen. The ultimate load (kgf) was obtained directly from the load-deformation curve.

Patient study

Patients: Spinal microarchitecture was examined in 82 postmenopausal women (55–76 years old, 65.3 ± 4.8 years) with MDCT scanning. Microstructure parameters were compared between 39 women who experienced their first spinal fracture during the previous 6 months (age: 66.2 ± 3.8 years old) and 43 women without fracture (age: 64.4 ± 5.5 years old) to assess the correlation between these parameters and fracture. Spinal fracture was defined according to the criteria proposed by Genant et al.[14] (i.e., vertebral deformity was considered as a fracture when at least a 20% reduction in anterior, middle, and/or posterior height and a 10% reduction in area were observed). Individuals who had had an osteoporotic fracture 6 months or more before the study were excluded, because bone structure would have been altered by the fracture. None of the postmenopausal women had received drugs affecting bone mass or bone metabolism within 6 months before the study. Nagasaki University ethics committee approved the protocol, and all subjects (i.e., fracture cases and controls) gave their informed consent.

BMD measurements: BMD of the lumbar spine (L_2–L_4) in antero-posterior (AP) projection was determined using DXA_1 and fractured vertebrae were excluded from the analysis. The obtained values were expressed as units of grams per centimeter squared for the projected area. Expert-EL (Lunar Corp., Madison, WI, USA) was used to measure the BMD of the lumbar spine. The CV (short-term precision) for L_2–L_4 was 1.1%.

To obtain volumetric BMD data by QCT, we scanned the patients simultaneously with MDCT using a bone mineral reference phantom (B-MAS2000; KYOTOKAGAKU Co.,

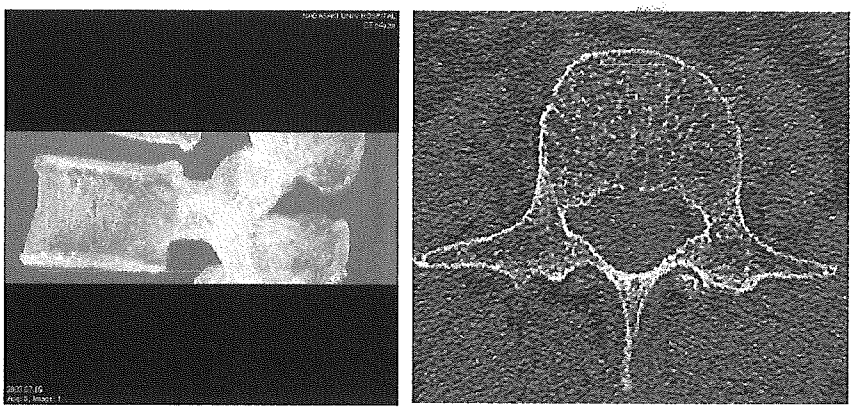

(A) (B)

FIG. 2. ROI for analysis of trabecular microstructure by MDCT. (A) The whole third lumbar spine including both endplates was scanned by MDCT. (B) The volume of interest (VOI) of 65 × 65 pixels in plane was defined in the anterior part of the spongiosa (delimited by the square) to avoid cortex and the basivertebral foramen.

Kyoto, Japan) containing calibration objects with equivalent densities of 0, 50, 100, 150, and 200 mg/cm^3 calcium hydroxyapatite. Reconstructed stacked 3D volume data of the vertebral body with reference phantom were used for the determination of volumetric BMD. VOI was defined in the same region for microstructure measurement of the reconstructed vertebral CT image.

Imaging by MDCT and structure analysis: The whole third lumbar spine including both endplates was scanned by MDCT, as shown in Fig. 2A. Patients were in the supine position for horizontal scanning of the vertebral body. The vertebral body was scanned under the appropriate X-ray condition, which was determined in the ex vivo cadaver study as described above. For the analysis of microstructure, the size of the VOI of 65 × 65 pixels in plane was defined (Fig. 2B); the total number of slices varied according to the size of the vertebral body. The VOI was defined manually within the internal part of the cancellous bone to avoid the cortex, the basivertebral foramen, and both endplates. The midline of the VOI in the *x*-axis in the axial image was in the center of the vertebral body, and the frontal edge on both sides of the VOI was just behind the cortex. The average number of slices was 43.8 ± 5.3 (range, 28–52 slices).

The procedure for structure analysis was the same as that for the cadaver specimen study described above. Samples from three patients were scanned five times on different days, using manually defined VOI; the precision was confirmed by the same operator. Precision of measurements of microstructure parameters was 0.67% for fractal dimension, 0.84% for Tb.Th, 1.13% for SMI, 2.04% for DA, 6.57% for Tb.N, 7.13% for BV/TV, 7.36% for Tb.Sp, and 12.30% for Euler's number.

Statistical analysis

Data analysis was performed with the software statistical package for Social Science, SPSS (SPSS, Chicago, IL, USA). Mean and SD of microstructure parameters and BMD were calculated for the postmenopausal women with or without fracture. The significance of differences between the two groups was calculated by ANOVA and posthoc test (Fisher's protected least significant difference [PLSD]), at the 95% significance level. Correlations of microstructure parameters or BMD with age or body weight of the subjects and correlations between microstructure parameters and BMD were assessed using linear regression analysis. Area under the curve (AUC) in receiver operator characteristic (ROC) analysis was generated to determine the diagnostic efficacy for detection of fracture cases. Additionally, the ORs per SD were calculated by logistic regression analysis to provide an estimate for the discriminatory capability of each variable for spinal fracture, as a single parameter or in combination with DXA or QCT value.

RESULTS

Specimen study

Optimal conditions for MDCT scanning: To determine the optimal conditions for MDCT scanning, we obtained vertebral specimens from cadavers and scanned them by both μCT (Fig. 1A) and MDCT (Figs. 1B–1D). Microstructure parameters were calculated at threshold values of 1120, 1200, and 1280 to binarize bone CT images. These values of threshold were numbers on a scale from 0 to 4290 according to linear attenuation, which has no units. As shown in Fig. 1 (right), at all three threshold levels, BV/TV obtained by μCT revealed the highest correlation with app BV/TV by MDCT at 300 mAs (r = 0.979, $p < 0.005$ at a threshold value of 1200).

When scanned at 0.5 mm thickness, 71-mm scan length, 0.8 feed/rotation, and 120 kVp, weighted CT dose indices (CTDIw) were 46.3 mGy for 200 mAs, 59.1 mGy for 250 mAs, and 77.1 mGy for 300 mAs.

Correlation between microstructure parameters and biomechanical properties: To examine whether microstructure parameters correlate with biomechanical properties, another set of four specimens were obtained from the femoral head at surgery and subjected to compression test after scanning by μCT and MDCT. As shown in Fig. 3, microstructure parameters obtained by MDCT revealed a high correlation with ultimate load (kgf); a significant correlation with the ultimate load was obtained for app BV/TV ($p < 0.05$), SMI ($p < 0.05$), and app Th.N ($p < 0.05$).

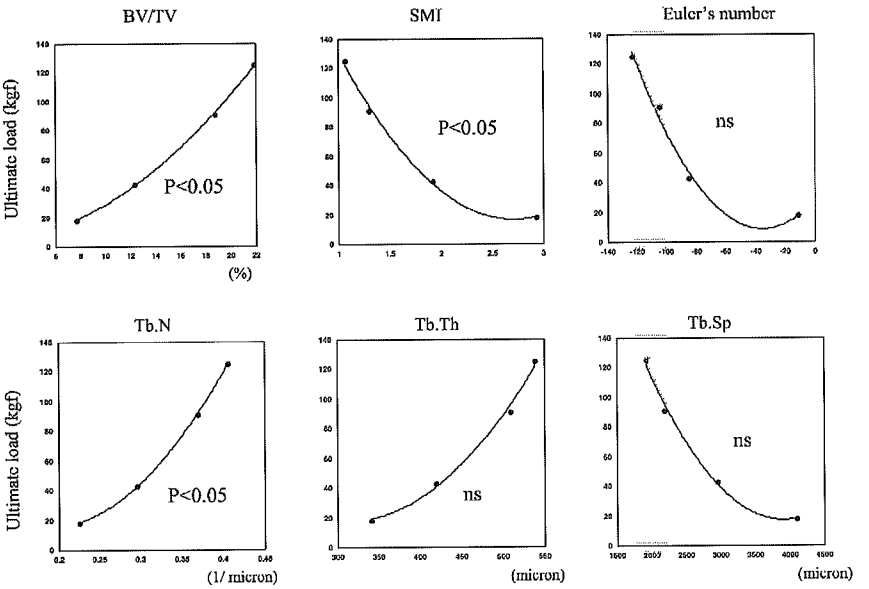

FIG. 3. Correlation between microstructure parameters and bone strength. Ten-millimeter cubic specimens were obtained from the femoral head of four individuals and scanned by μCT and MDCT. Structure analysis was performed as described in the Materials and Methods section. The specimens were subjected to biomechanical test, and the ultimate load was obtained from the load-deformation curve. Shown are significant correlations between microstructure parameters obtained by MDCT and bone strength. p values are shown for each parameter.

Patient study

Association of microstructure parameters with prevalent spinal fracture: To examine the use of trabecular microarchitecture information obtained by MDCT scanning for the assessment of fracture, we compared the microstructure parameters derived from MDCT images between 43 women without fracture (age: 64.4 ± 5.5 years old) and 39 women with a recent spinal fracture (age: 66.2 ± 3.8 years old). As shown in Table 1, there was no significant difference in age, age at menopause, body height (BH), or body weight (BW) between these two groups of women.

Figures 4A–4F show representative 2D (Figs. 4A and 4B), its binarized 2D (Figs. 4C and 4D), and 3D (Figs. 4E and 4F) MDCT images of the third lumbar vertebra of a 62-year-old woman without vertebral fracture (Figs. 4A, 4C, and 4E) and those of a women of the same age with a fracture in the thoracic spine (Figs. 4B, 4D, and 4F).

Table 1 summarizes the results of microstructure parameters, as well as areal (by DXA) and volumetric (by MDCT) BMD values in the two groups of women. Areal BMD by DXA was significantly lower in postmenopausal women with a fracture than in those without one (0.836 ± 0.191 versus 0.925 ± 0.161 g/cm^2, $p < 0.05$). Among the microstructure indices obtained by MDCT, app BV/TV, app Tb.N, app Tb.Th, and fractal dimension were significantly lower; whereas app Tb.Sp, SMI, Euler's number, and DA were significantly higher in women with a fracture than in those without a fracture (Table 1). Volumetric BMD determined by MDCT was also significantly lower in postmenopausal women with a fracture (72.0 ± 18.5 versus 103.9 ± 23.5 mg/cm^3, $p < 0.0001$).

Table 2 shows the correlation of microstructure parameters with BMD values obtained by DXA and QCT. Most microstructure parameters were more highly correlated with volumetric BMD by QCT than with areal BMD by DXA.

ROC analysis was performed to determine the diagnostic value of microstructure parameters with respect to fracture (Table 3). The highest AUC value was obtained for SMI (0.928), which was significantly higher than that for areal BMD by DXA (0.647) or volumetric BMD by MDCT (0.870). AUC values of Euler's number (0.857) and app Tb.Sp (0.818) were similar to that value of volumetric BMD, and significantly exceeded that of areal BMD by DXA. The ORs for the association of SMI (16.0), app BV/TV (13.6), Euler's number (13.1), app Tb.Sp (7.4), fractal dimension (7.4), app Tb.N (6.6), and app Tb.Th (5.5) with fracture were higher than the OR for that of areal BMD by DXA with it (4.8); the ORs for SMI, app BV/TV, and Euler's number exceeded that ratio of volumetric BMD (12.7). Multivariate regression analysis showed significant correlations of SMI (R^2 = 0.329, $p < 0.0001$) and Tb.Th (R^2 = 0.154, $p < 0.005$), as well as volumetric BMD (R^2 = 0.159, $p < 0.005$), with fracture (Table 4). Combining areal or volumetric BMD data with some microstructural parameters further increased R^2 values compared with BMD alone (Table 4).

Table 5 shows the correlations of spinal microarchitecture or BMD with age and BW. Most microstructure parameters and volumetric BMD by MDCT correlated with age, especially SMI, Euler's number, and app BV/TV, whereas areal BMD values by DXA showed a moderate correlation with both age and BW.

DISCUSSION

The purpose of this study was to evaluate the diagnostic value of in vivo analysis of spinal trabecular microstructure, focusing on its association with prevalent spinal fracture. Compared with postmenopausal women without a spinal fracture, those with one had a smaller trabecular bone fraction (app BV/TV: 36.1 versus 26.2) in association with fewer

TABLE 1. COMPARISON OF VERTEBRAL MICROSTRUCTURAL PARAMETERS BETWEEN TWO GROUPS WITHOUT AND WITH FRACTURE

	Without fracture (n = 43)	*With fracture (n = 39)*	*p (by t-test)*
Background data			
Anthropometric data			
Age (years)	64.4 ± 5.5	66.2 ± 3.8	NS
Age at menopause (years)	50.3 ± 2.8	48.9 ± 4.2	NS
Body height (cm)	152.3 ± 4.7	150.1 ± 7.2	NS
Body weight (kg)	52.8 ± 7.3	50.1 ± 7.8	NS
Areal BMD by DXA (g/cm^2)	0.925 ± 0.161	0.836 ± 0.191	0.05
MDCT data			
Microstructure parameters			
App BV/TV (%)	36.1 ± 7.0	26.1 ± 8.5	<0.0001
App Tb.N ($1/mm^3$)	0.97 ± 0.09	0.78 ± 0.20	<0.0001
App Tb.Th (μm)	368.3 ± 46.1	335.8 ± 46.2	0.005
App Tb.Sp (μm)	667 ± 129	1064 ± 439	<0.0001
Structure model index	1.87 ± 0.48	2.70 ± 0.38	<0.0001
Euler's number	−1037 ± 375	−457 ± 404	<0.0001
Fractal dimension	2.52 ± 0.06	2.41 ± 0.18	0.0005
Degree of anisotropy	1.44 ± 0.15	1.58 ± 0.35	0.05
Volumetric BMD (mg/cm^3)	103.9 ± 23.5	72.0 ± 18.5	<0.0001

Data are shown as mean ± SD.

app BV/TV, apparent bone volume fraction; app Tb.N, apparent trabecular number; app Tb.Th, apparent trabecular thickness; app Tb.Sp, apparent trabecular separation; NS, not significant.

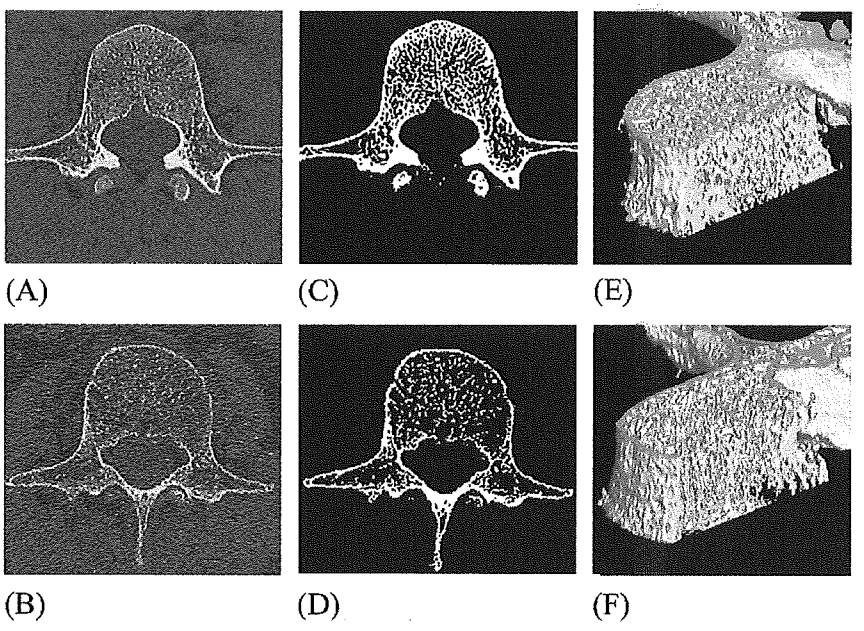

FIG. 4. Representative 2D and 3D MDCT images of the third lumbar spine. (A and B) 2D and (E and F) 3D MDCT images of the third lumbar spine were obtained from (A and E) a 62-year-old woman without vertebral fracture and (B and F) a woman of the same age with a vertebral fracture in her thoracic spine. (C and D) Binarized images are also shown.

trabeculae (app Tb.N: 0.97 versus 0.78), more rodlike structure (SMI: 1.87 versus 2.70), and lower connectivity (Euler's number: −1037 versus −457). The ORs of microstructure parameters, such as SMI, Euler's number, and app BV/TV, for association with prevalent fracture were much higher than that ratio for association of areal BMD by DXA with it. SMI and Euler's number, which represent nonmetric features of trabecular structure, would seem to be more useful than metric parameters such as app Tb.N, app Tb.Th, or app Tb.Sp. It is an advantage of the MDCT scanning system that, in addition to assessing these 3D microstructure parameters, volumetric BMD values can be obtained at the same time by using a reference phantom; these values correlate highly with the presence of fracture.

In vivo analysis of trabecular microstructure has been studied using conventional radiography, high-resolution CT, and high-resolution MRI. Conventional radiography has a spatial resolution of up to 40 μm; however, it delivers projectional images of the trabecular structure. Conventional high-resolution CT with spatial resolution of 400 μm shows only structural texture, because the trabecular structure is subjected to partial-volume effects. With the use of

TABLE 2. CORRELATIONS BETWEEN MICROSTRUCTURAL PARAMETERS AND BMD

Structure parameters by MDCT	*Volumetric BMD by QCT*		*Areal BMD by DXA*	
	R^2	*p*	R^2	*p*
App BV/TV (%)	0.645	0.0001	0.128	0.005
Structure model index	0.514	0.0001	0.151	0.0005
App Tb.Th (μm)	0.487	0.0001	0.083	0.01
Euler's number	0.433	0.0001	0.125	0.005
App Tb.N (1/mm^3)	0.428	0.0001	0.104	0.005
App Tb.Sp (μm)	0.350	0.0001	0.045	NS
Fractal dimension	0.311	0.0001	0.213	0.0001
Degree of anisotropy	0.084	0.01	0.034	NS

app BV/TV, apparent bone volume fraction; app Tb.Th, apparent trabecular thickness; app Tb.N, apparent trabecular number; app Tb.Sp, apparent trabecular separation; NS, not significant.

TABLE 3. ROC ANALYSIS AND ORS OF MICROSTRUCTURAL PARAMETERS FOR THEIR ASSOCIATION WITH SPINAL FRACTURE

Measurements	*AUC (ROC)*	*p*	*OR (95% CI)*	*p*
MDCT				
Microstructural parameters				
Structural model index	0.928 ± 0.027	0.0001	16.0 (5.3–48.4)	0.0001
App BV/TV (%)	0.811 ± 0.048	0.0001	13.6 (4.3–42.4)	0.0001
Euler's number	0.857 ± 0.043	0.0001	13.1 (4.5–38.1)	0.0001
App Tb.Sp (μm)	0.818 ± 0.048	0.0001	7.4 (2.8–19.8)	0.0001
Fractal dimension	0.735 ± 0.059	0.0001	7.4 (2.6–20.7)	0.0005
App Tb.N (1/mm^3)	0.810 ± 0.049	0.0001	6.6 (2.5–17.4)	0.0005
App Tb.Th (μm)	0.674 ± 0.059	0.01	5.5 (1.6–18.5)	0.01
Degree of anisotropy	0.627 ± 0.063	0.05	3.5 (1.2–10.2)	0.05
Volumetric BMD (mg/cm^3)	0.870 ± 0.040	0.0001	12.7 (4.4–36.4)	0.0001
DXA areal BMD (g/cm^2)	0.647 ± 0.062	0.05	4.8 (1.5–14.8)	0.05

Data are shown as mean ± SD.
app BV/TV, apparent bone volume fraction; app Tb.Sp, apparent trabecular separation; app Tb.N, apparent trabecular number; app Tb.Th, apparent trabecular thickness.

TABLE 4. CORRELATION OF MICROSTRUCTURE PARAMETERS AND BMD WITH FRACTURE

vBMD with microstructure parameters			*aBMD with microstructure parameters*		
Measures	R^2	*p*	*Measures*	R^2	*p*
vBMD	0.366	0.0001	aBMD	0.061	0.0251
SMI	0.486	0.0001	SMI	0.486	0.0001
Tb.Th	0.112	0.0021	Euler's number	0.362	0.0001
vBMD + SMI	0.508	0.0001	aBMD + SMI	0.486	0.0001
vBMD + SMI + Tb.T	0.551	0.0001	aBMD + SMI + Euler's number	0.506	0.0001

Correlation with prevalent vertebral fracture was assessed by multivariate regression analysis.
vBMD, volumetric BMD; aBMD, areal BMD.

high-resolution CT in vivo, analysis of trabecular structure such as connectivity from a skeletonized representation of the trabecular network,[4] parameters derived from run-length encoding,[6] and number or area of holes in trabecular structure[15] have been reported. Their images had a slice thickness of 1.5 mm and the FOV was reduced to yield an image matrix with a pixel size of 0.31 mm. A good relationship between texture parameters calculated from high-resolution CT images and biomechanical properties has also been reported.[5] However, this spatial resolution only provides characteristics of trabecular structure, and 2D image has limited reproducibility among follow-up examinations.

With the recent advances in MRI hardware and software, it has become possible to obtain higher resolution MR images of trabecular bone[16–22] with in-plane resolutions as high as 150 μm and slice thicknesses of 280 μm in vivo.[23] MRI has an advantage of nonionization, and trabecular microstructure obtained in vivo by using high-resolution MR has been shown to be useful in predicting prevalent spinal fractures. Structural parameters of the distal radius with a 3D spin-echo sequence (voxel size of 137 × 137 × 500 μm^3) in 36 female patients were reported to provide a better index than the BMD of the distal radius.[24] 3D gradient-echo sequence (voxel size of 156 × 156 × 500 μm^3) could discriminate between groups with and without a recent hip

TABLE 5. CORRELATIONS OF MICROSTRUCTURAL PARAMETERS BY MDCT WITH AGE OR BODY WEIGHT

	Vs. age (years)		*Vs. body weight (kg)*	
	R^2	*p*	R^2	*p*
Microstructure parameters				
App BV/TV (%)	0.114	0.0005	0.029	NS
App Tb.N (1/mm^3)	0.122	0.005	0.147	0.0005
App Tb.Th (μm)	0.099	0.005	0.030	NS
App Tb.Sp (μm)	0.081	0.01	0.125	0.005
Structure model index	0.181	0.0001	0.048	0.05
Euler's number	0.185	0.0001	0.068	0.05
Fractal dimension	0.049	0.05	0.030	NS
Degree of anisotropy	0.005	NS	0.130	0.001
BMD				
Areal BMD by DXA (g/cm^2)	0.091	0.01	0.072	0.05
Volumetric BMD by MDCT (mg/cm^3)	0.118	0.005	0.001	NS

app BV/TV, apparent bone volume fraction; app Tb.N, apparent trabecular number; app Tb.Th, apparent trabecular thickness; app Tb.Sp, apparent trabecular separation; NS, not significant.

fracture.[21] A disadvantage of high-resolution MRI in vivo, however, is the relatively long acquisition time of up to 10 ± 20 minutes. A small FOV is required to obtain a high signal-to-noise ratio in the fast gradients with optimized coils. Because of these prerequisites and motion artifacts in the axial skeleton, application of high-resolution MRI is currently limited to peripheral sites such as phalanges, calcaneus, and distal radius.[19,20,25–27] Vertebral fracture is the most common osteoporotic fracture, and the presence of fracture indicates a greater risk for future fracture, independently of BMD.[28] The direct assessment of vertebral microstructure, as reported here, can be expected to provide greater sensitivity for assessing the risk of spinal fracture.

To our knowledge, there has been no report on in vivo analysis of microstructure by MDCT. Several specimen studies showed the capability to depict microstructure by MDCT in comparison with contact radiography[16] or μCT.[17] Although MDCT is the only available technique to analyze vertebral microstructure in vivo, high radiation exposure cannot be avoided. The radiation dose for DXA is small (0.08 ± 4.6 mSv). Fan beam DXA with increased resolution requires an increased radiation dose (6.7 ± 31 mSv), but this dose is smaller than that for QCT (25 ± 360 mSv).[29] In a study comparing radiation doses between single-detector row CT and MDCT, a 28% higher radiation dose was needed within the scanned volume for the latter at a constant noise level.[30] In this study, we evaluated the image quality of trabecular microstructure as a function of radiation exposure dose by using excised human vertebrae. Within the limits of clinically available radiation sets, MDCT at 300 mAs provided the best image quality and showed the highest correlation with the μCT data. As the reference level for CT examination of the abdomen (CTDIw) of adult patients is 35 mGy (according to European Commission 1999), the CTDIw for our current MDCT scanning at 300 mAs was 77.1 mGy. This radiation dose would be acceptable for a once-a-year study on postmenopausal women. On further advancement of the technology, a reduction in the radiation dose and higher resolution with a higher signal-to-noise ratio would be expected to make this method an even more useful diagnostic tool. In fact, the CTDIw for a new 16-detector row CT apparatus is 19.7 mGy, and advanced CT technology is expected to provide higher-resolution CT images. In the future, finite element analysis (FEA) may also be applied to 3D MDCT data for assessment of biomechanical properties,[31,32] and together this combination should provide a powerful tool for early evaluation of fracture risk.

In conclusion, 3D imaging of trabecular microstructure can be performed by using clinical MDCT at a high spatial resolution, and microstructure parameters derived from these images, especially those related to the shape of trabecular structures and connectivity, are more useful than spinal DXA for the assessment of fracture risk.

ACKNOWLEDGMENTS

The authors thank Tomoko Nakata and Takako Shimogama (Division of Radiology, Nagasaki University Hospital) and Jun Kono (Department of Radiology, Nagasaki Saiseikai Hospital) for CT scanning and analysis of trabecular structure. This work was supported in part by the Program for Promotion of Fundamental Studies in Health Science from Pharmaceuticals and Medical Device Agency (Pmda) of Japan (MF-14 to MI) and by a Health and Labour Sciences Research Grant (Comprehensive Research on Aging and Health) from the Ministry of Health, Labour and Welfare of Japan (to MI and HO).

REFERENCES

1. Siris ES, Chen Y-T, Abbott TA, Barrett-Connor E, Miller PD, Wehren LE, Berger MC 2004 Bone mineral density thresholds for pharmacological intervention to prevent fractures. Arch Intern Med **164**:1108–1112.
2. Riggs BL, Melton LJ 2002 Bone turnover matters: The raloxifene treatment paradox of dramatic decreases in vertebral fractures without commensurate increases in bone density. J Bone Miner Res **17**:11–14.

3. Seeman E 2002 Pathogenesis of bone fragility in women and men. Lancet **359:**1841–1850.
4. Chevalier F, Laval-Jeantet A, Laval-Jeantet M, Bergot C 1992 CT image analysis of the vertebral trabecular network in vivo. Calcif Tissue Int **51:**8–13.
5. Link TM, Majumdar S, Lin J, Augat P, Gould R, Newitt D, Ouyang X, Lang T, Mathur A, Genant HK 1998 Assessment of trabecular structure using high-resolution CT images and texture analysis. J Comput Assist Tomogr **22:**15–24.
6. Ito M, Ohki M, Hayashi K, Yamada M, Uetani M, Nakamura T 1995 Trabecular texture analysis of CT images in the relationship with spinal fracture. Radiology **194:**55–59.
7. Ruegsegger P, Koller B, Mueller R 1996 A microtomographic system for the non-destructive evaluation of bone architecture. Calcif Tissue Int **58:**24–29.
8. Mueller R, Hahn M, Vogel M, Delling G, Ruegsegger P 1996 Morphometric analysis of non-invasively assessed bone biopsies: Comparison of high-resolution computed tomography and histologic sections. Bone **18:**215–220.
9. Hildebrand T, Ruegsegger P 1997 A new method for the model-independent assessment of thickness in three-dimensional images. J Microsc **185:**67–75.
10. Parfitt AM, Drezner MK, Glorieux FH, Kanis JA, Malluche H, Meunier PJ, Ott SM, Recker RR 1987 Bone histomorphometry: Standardization of nomenclature, symbols, and units. Report of the ASBMR Histomorphometry Nomenclature Committee. J Bone Miner Res **2:**595–610.
11. Fazzalari NL, Parkinson IH 1996 Fractal dimension and architecture of trabecular bone. J Pathol **178:**100–105.
12. Odgaard A, Gundersen HJ 1993 Quantification of connectivity in cancellous bone, with special emphasis on 3-D reconstructions. Bone **14:**173–182.
13. Harrigan TP, Mann RW 1984 Characterization of microstructural anisotropy in orthotropic materials using a second rank tensor. J Mater Sci **19:**761–767.
14. Genant HK, Wu CY, vanKuijk C, Nevitt M 1994 Vertebral fracture assessment using a semi-quantitative technique. J Bone Miner Res **8:**1137–1148.
15. Gordon CL, Lang TF, Augat LP, Genant HK 1998 Image-based assessment of spinal trabecular bone structure from high-resolution CT images. Osteoporos Int **8:**317.
16. Link TM, Vieth V, Stehling C, Lotter A, Beer A, Newitt D, Majumdar S 2003 High-resolution MRI vs multislice spiral CT: Which technique depicts the trabecular bone structure best? Eur Radiol **13:**663.
17. Issever AS, Vieth V, Lotter A, Meier N, Laib A, Newitt D, Majumdar S, Link TM 2002 Local differences in the trabecular bone structure of the proximal femur depicted with high-spatial-resolution MR imaging and multisection CT. Acad Radiol **9:**1395.
18. Gordon CL, Webber CE, Christoforou N, Nahmias C 1997 In vivo assessment of trabecular bone structure at the distal radius from high-resolution magnetic resonance images. Med Phys **24:**585–593.
19. Majumdar S, Genant HK, Grampp S, Newitt DC, Truong V-H, Lin JC, Mathur A 1997 Correlation of trabecular bone structure with age, bone mineral density and osteoporotic status: In vivo studies in the distal radius using high resolution magnetic resonance imaging. J Bone Miner Res **12:**111–118.
20. Link TM, Majumdar S, Augat P, Lin JC, Newitt D, Lu Y, Lane NE, Genant HK 1998 In vivo high resolution MRI of the calcaneus: Differences in trabecular structure in osteoporosis patients. J Bone Miner Res **13:**1175–1182.
21. Majumdar S, Link TM, Augat P, Lin JC, Newitt D, Lane NE, Genant HK 1999 Trabecular bone architecture in the distal radius using magnetic resonance imaging in subjects with fractures of the proximal femur. Osteoporos Int **10:**231–239.
22. Majumdar S, Kothari M, Augat P, Newitt DC, Link TM, Lin JC, Lang T, Lu Y, Genant HK 1998 High-resolution magnetic resonance imaging: Three-dimensional trabecular bone architecture and biomechanical properties. Bone **22:**445–454.
23. Majumdar S, Newitt D, Mathur A, Osman D, Gies A, Chiu E, Lotz J, Kinney J, Genant H 1996 Magnetic resonance imaging of trabecular bone structure in the distal radius: Relationship with X-ray tomographic microscopy and biomechanics. Osteoporos Int **6:**376–385.
24. Wehrli F, Hwang S, Ma J, Song H, Ford J, Haddad J 1998 Cancellous bone volume and structure in the forearm: Noninvasive assessment with MR microimaging and image processing. Radiology **206:**347–357.
25. Lin J, Amling M, Newitt D, Selby K, Delling G, Genant H, Majumdar S 1996 Heterogeneity of trabecular bone structure in the calcaneus using high resolution magnetic resonance imaging (MRI). Osteoporos Int **8:**16–24.
26. Link T, Majumdar S, Lin J, Newitt D, Augat P, Ouyang X, Mathur A, Genant H 1998 A comparative study of trabecular bone properties in the spine and femur using high resolution MRI and CT. J Bone Miner Res **13:**122–132.
27. Kuehn B, Stampa B, Heller M, Glueer C 1997 In vivo assessment of trabecular bone structure of the human phalanges using high resolution magnetic resonance imaging. Osteoporos Int **7:**291.
28. Ross PD, Genant HK, Davis JW, Miller PD, Wasnich RD 1993 Predicting vertebral fracture incidence from prevalent fractures and bone density among non-black, osteoporotic women. Osteoporos Int **3:**120–126.
29. Njeh CF, Fuerst T, Hans D, Blake GM, Genant HK 1999 Radiation exposure in bone mineral density assessment. Appl Radiat Isot **50:**215.
30. Thornton FJ, Paulson EK, Yoshizumi TT, Frush DP, Nelson RC 2003 Single versus multi-detector row CT: Comparison of radiation doses and dose profiles. Acad Radiol **10:**379.
31. van Rietbergen B, Weinans H, Huiskes R, Odgaard A 1995 A new method to determine trabecular bone elastic properties and loading using micromechanical finite-element models. J Biomech **28:**69–81.
32. Ito M, Nishida A, Koga A, Ikeda S, Shiraishi A, Uetani M, Hayashi K, Nakamura T 2002 Contribution of trabecular and cortical components to the mechanical properties of bone and their regulating parameters. Bone **31:**351–358.

Address reprint requests to:
Masako Ito, MD
Division of Radiology
Nagasaki University Hospital
Nagasaki 852-8501, Japan
E-mail: masako@net.nagasaki-u.ac.jp

Received in original form February 16, 2005; revised form June 4, 2005; accepted June 16, 2005.

Osteoporos Int (2005) 16: 1042–1048
DOI 10.1007/s00198-004-1802-3

ORIGINAL ARTICLE

Effects of risedronate on trabecular microstructure and biomechanical properties in ovariectomized rat tibia

Masako Ito · Akifumi Nishida · Kiyoshi Aoyagi
Masataka Uetani · Kuniaki Hayashi · Masahiro Kawase

Received: 19 August 2003 / Accepted: 21 October 2004 / Published online: 12 February 2005

Abstract We determined the effect of risedronate on the trabecular microstructure of ovariectomized rat tibiae, using micro-computed tomography, in order to investigate how changes in microstructure contribute to biomechanical properties. Fifty 18-week-old rats underwent sham operation ($n=10$) or ovariectomy (OVX) ($n=40$). The OVX rats were further divided into four groups ($n=10$ for each group) and treated with risedronate at doses of 0, 0.1, 0.5 or 2.5 mg/kg for 9 months. OVX caused deterioration of three-dimensional trabecular microstructure, notably structure model index (SMI) and connectivity density, while treatment of OVX rats with risedronate at 0.5 and 2.5 mg/kg improved those deleterious microstructural changes. Biomechanical property, as assessed by finite element analysis (FEA), correlated significantly with trabecular bone volume fraction (BV/TV), and the correlation further increased substantially when microstructural parameters were added, especially SMI and connectivity density, with risedronate therapy. Thus, it is suggested that, in addition to increasing bone mass, risedronate improves biomechanical property by maintaining a plate-like structure as well as connectivity of trabeculae.

Keywords Biomechanical property · Connectivity · Finite element analysis (FEA) · Microstructure · Risedronate

M. Ito (✉) · A. Nishida · M. Uetani · K. Hayashi
Department of Radiology, Nagasaki University
School of Medicine, 1-7-1 Sakamoto, 852-8501
Nagasaki, Japan
E-mail: masako@net.nagasaki-u.ac.jp
Tel.: +81-95-8497354
Fax: +81-95-8497357

K. Aoyagi
Department of Public Health, Nagasaki University
School of Medicine, Nagasaki, Japan

M. Kawase
Drug Analysis & Pharmacokinetics Research Laboratories,
Pharmaceutical Research Division, Takeda Chemical Industries
Ltd., Osaka, Japan

Introduction

According to meta-analyses of clinical trials of anti-resorptive agents, with regard to the relative risk of vertebral fractures as a function of a change in bone mineral density (BMD), most of the efficacy has been explained by an 8% increase in spinal BMD, which produced a 41% risk reduction [1]. Risedronate has been reported to decrease the risk of the first new vertebral fracture by up to 70% in the first year of treatment in postmenopausal women [2].

In animal studies the effects of risedronate on trabecular bone mass and architecture have been studied in the vertebrae of ovariectomized (OVX) minipigs [3]. Although preservation of trabecular microstructure is believed to contribute to bone strength [3, 4], the relationship between micro-architecture and biomechanical properties after treatment with anti-osteoporotic agents is not fully understood.

The purpose of this study is to investigate how treatment with risedronate changes trabecular microstructure and how these changes in microstructure contribute to biomechanical properties, using ovariectomized rat tibia. We employed three-dimensional (3D) micro-computed tomography (micro-CT) to determine changes in trabecular microstructure, as well as micro-finite element analysis (FEA) to assess biomechanical properties.

Materials and methods

Reagents

Risedronate (NE-58095) was obtained from Ajinomoto Co. Inc., (Tokyo, Japan) as characterized by Process Development, Proctor and Gamble Pharmaceuticals, Norwich, New York, USA. It was dissolved in sterile physiological saline.

Animals

Nine-week-old female Sprague–Dawley rats were purchased from Charles River Japan, (Shiga, Japan) and acclimated under standard laboratory conditions at 22±2°C and 50±10% humidity. Powder food (CE-2, Clea, Japan) was available, ad libitum, during the acclimation period, and water was available, ad libitum, from an automatic water supply apparatus (Edstrom Industries).

Experiment design

Sham-operation ($n=10$) or OVX ($n=40$) was performed when the rats were 18 weeks of age. The OVX rats were divided into four groups ($n=10$ for each group), 1 week after surgery. Sham and OVX vehicle groups received vehicle (isotonic sodium chloride solution) orally. Risedronate was administered orally by catheter at 0.1, 0.5, and 2.5 mg/kg b.w. seven times per week. The vehicle and the drug were given on the same days, and the treatment was continued for 9 months. These animal studies were carried out in accordance with Shin Nippon Biochemical Laboratories' ethical guidelines for animal care, and the experimental protocols were approved by the animal care committee of the institution.

When the study had been completed the animals' left tibiae were removed and stored at −20°C for the assessment of trabecular microstructure.

Micro-computed tomography

The micro-CT apparatus (μCT40) used in this study was provided by SCANCO Medical (Basserdorf, Switzerland) [5]. Details of an earlier model, the micro-CT scanner (μCT20) have been described previously [6]. The μCT40 is able to provide a high scan speed (9 s to 120 s per slice), using a cone beam, and the highest spatial resolution of 6 μm voxel size (10% MTF at 8.8 μm). This system has a micro-X-ray source with 5 μm spot-size (30–70 keV, 0.16 mA) directed towards the sample. The X-ray beam is analyzed with a plane detector (CCD array; 1,024×46 elements). The process is piloted by an Alpha DS10 workstation (Compaq Computer Corporation, Delaware, USA), and an open VMS system in a cluster configuration was used to perform 3D analysis. Each tibia was positioned to be scanned cranio-caudally, using 360 slices with 8 μm increments (approximately 2.9 mm) below 0.5 mm distance from the growth plate. To obtain the original 3D image of the proximal tibia [7], we used a threshold value of 275 permille of maximal gray scale value to binarize the spongiosa and cortex in this analysis system [8]. The threshold value of 275 permille was selected based on our investigation to separate bone and other components adequately, using discrimination analysis.

Measurement of trabecular bone mass and microstructure

On the original 3D image, morphometric indices were directly determined from the binarized volume of interest (VOI), which was defined in the whole spongiosa of the proximal tibia (VOI-1). Trabecular bone volume fraction (BV/TV) was calculated with bone volume (BV) and total tissue volume (TV). Mean trabecular thickness (Tb.Th) was determined from local thickness by the distance-transformation method [9]. We calculated trabecular separation (Tb.Sp) by applying the same technique that was used for the direct thickness calculation to the non-bone parts of the 3D image. We calculated trabecular number (Tb.N) by taking the inverse of the mean distance between the middle axes of the structure (the ridge number density) [10].

The structure model index (SMI) is a parameter that quantifies the characteristic form of a three-dimensionally described structure in terms of the number of plates and rods that compose the structure [11]. The degree of anisotropy (DA) defines the direction and magnitude of the preferred orientation of trabeculae and uses the ratio between the maximum and minimum radii of the mean intercept length (MIL) ellipsoid [12]. Connectivity density is a topological parameter that estimates the number of trabecular connections per cubic millimeter. The perforation of plates without the breaking of trabecular connections would artificially increase the connectivity density [13, 14]. The software of 3D microstructure analysis was provided by SCANCO Medical (Basserdorf, Switzerland) [5].

Finite element analysis

The effect of risedronate on biomechanical properties of bone was investigated by FEA in this study, since the compression biomechanical test is not usually performed on the trabecular bone compartment of the tibia. We applied the FEA programs to analyze the relationship between the microstructure and its biomechanical strength.

The cubic bone volume (152×152×152 voxels) was defined in the tibial spongiosa beneath the patella–tibial joint space (Fig. 2A). After the microstructural parameters had been calculated in this VOI (VOI-2), which was different from VOI-1, the data in VOI-2 were directly incorporated into a finite element (FE) model to determine, with the voxel-based FEA program, the elastic properties of the trabecular network. The 3D-binary image was used to generate an FE model by converting the pixels of the solid phase to correspondingly shaped eight-node brick elements [15].

Using a special-purpose FE-solver (SCANCO Medical FE-software, version 1.1), we simulated compression and shear tests in the three orthogonal directions. For these simulations the tissue elastic properties were set as linear elastic and isotropic, with a Young's modulus of

10 GPa and a Poisson's ratio of 0.3 [16]. The stiffness matrix was calculated from the results of the six simulations [17]. Then, we used an optimization procedure to find a new coordinate system aligned with the best orthogonal symmetry directions. The stiffness matrix was rotated to this new orthogonal coordinate system, and the Young's moduli ($E1$, $E2$, $E3$), as well as shear moduli ($G12$, $G13$, $G23$), were calculated in these principal directions. The matrix was sorted such that the Young's modulus in the primary direction ($E1$) represented the largest modulus and the third Young's modulus ($E3$) the smallest one: $E1 > E2 > E3$.

The number of elements in each data set ranged from 150,000 for low bone mass to more than 20 million for large bone mass. The calculations were performed with FEA software and provided direct and complete evaluation of the mechanical consequences of morphological changes, from which we could calculate tissue-level loading due to external forces. This system also provided sophisticated 3D rendering of the results. Figure 2B shows the 3D image of the original microstructure and Fig. 2C the corresponding 3D image of von Mises stress distribution.

Statistical analysis

Data are expressed as means ± standard deviation (SD). Each variable followed a Gaussian distribution. Statistical analysis was carried out by analysis of variance (ANOVA) and post-hoc test [Fisher's protected least significant difference (PLSD)], with Statistical Analysis System (SAS) software (SAS Institute, Cary, N.C., USA). A P value of < 0.05 was considered significant.

In order to investigate the contribution of each parameter or combination of parameters to bone biomechanical properties, we employed multiple linear regression analysis, with BV/TV and structural parameters as independent variables. The regression analysis produced a coefficient of multiple determination (R^2), which represents the proportion of variability in dependent parameters explained by independent variables in the model. $P < 0.05$ was considered significant.

Results

Effect of risedronate on trabecular microstructure

As illustrated in Fig. 1, and summarized in Table 1, OVX caused a marked deterioration in microstructure of the trabecular region of proximal tibiae, manifested as significant decreases in BV/TV ($P < 0.001$), Tb.Th ($P < 0.05$), Tb.N ($P < 0.05$) and connectivity density ($P < 0.001$), and increases in Tb.Sp ($P < 0.001$) and SMI ($P < 0.001$) compared to the sham-operated group. Risedronate at doses of 0.5 mg/kg or more reversed this microstructural deterioration significantly and in a dose-dependent manner in comparison with the OVX group ($P < 0.0001$ in all seven variables for trend). In the OVX rats treated with 2.5 mg/kg of risedronate, BV/TV, Tb.Th, Tb.N and connectivity density increased above the values of the sham group, while Tb.Sp, SMI and DA decreased to below the levels of the sham group (Table 1).

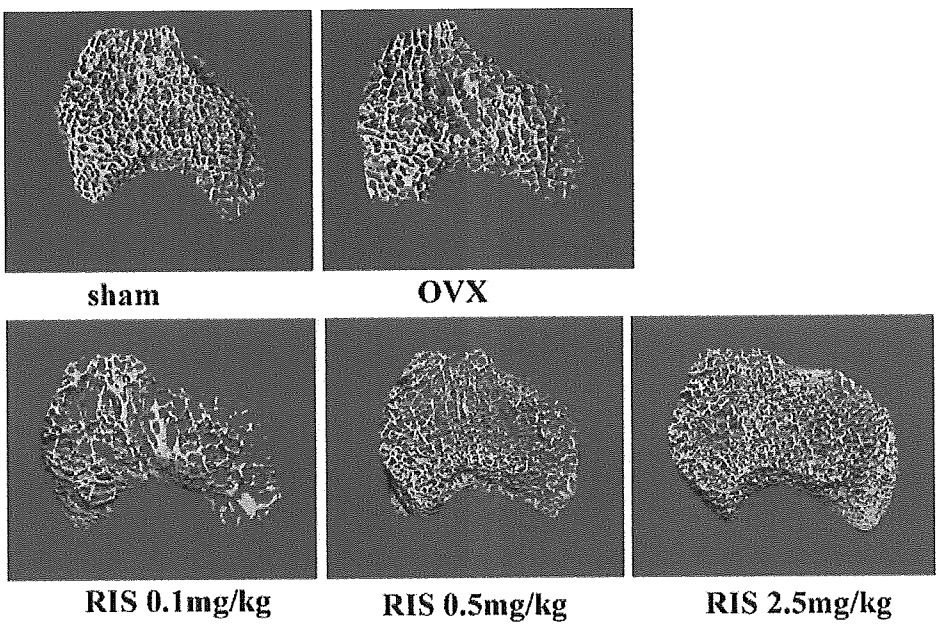

Fig. 1 Three-dimensional trabecular micro-CT images of tibia. Representative images of sham, OVX vehicle, and OVX rats treated with risedronate (0.1, 0.5, 2.5 mg/kg) are shown

Table 1 Microstructural parameters in the sham and OVX rats treated with risedronate (*ConnD* connectivity density, *NS* not significant)

Group	BV/TV (%)	*P*		Tb.Th (mm)	*P*		Tb.Sp (mm)	*P*		Tb.N (1/mm)	*P*	
Sham	0.30 ± 0.07			0.064 ± 0.005			0.161 ± 0.035			6.82 ± 1.60		
OVX vehicle	0.14 ± 0.07		†††	0.053 ± 0.010		†	0.344 ± 0.079		†††	3.33 ± 1.27		†††
OVX risedronate 0.1 mg/kg per day	0.16 ± 0.06	NS	††	0.061 ± 0.009	*	NS	0.292 ± 0.087	NS	††	3.96 ± 1.56	NS	†
OVX risedronate 0.5 mg/kg per day	0.20 ± 0.06	*	†	0.064 ± 0.007	**	NS	0.184 ± 0.045	***	NS	5.88 ± 1.72	**	NS
OVX risedronate 2.5 mg/kg per day	0.59 ± 0.21	***	††	0.076 ± 0.009	***	††	0.074 ± 0.043	***	†††	13.85 ± 3.99	***	†††

Group	SMI	*P*		DA	*P*		Conn.D (1/mm^3)	*P*	
Sham	0.72 ± 0.48			1.84 ± 0.12			180.0 ± 76.9		
OVX vehicle	1.79 ± 0.41		†††	1.98 ± 0.19		NS	34.3 ± 44.2		†††
OVX risedronate 0.1 mg/kg per day	1.92 ± 0.49	NS	†††	1.86 ± 0.18	NS	NS	63.6 ± 57.1	NS	††
OVX risedronate 0.5 mg/kg per day	−2.22 ± 0.49	***	†††	1.75 ± 0.08	**	NS	148.0 ± 111.7	**	NS
OVX risedronate 2.5 mg/kg per day	−3.93 ± 4.86	**	†	1.63 ± 0.05	***	†††	782.7 ± 55.2	***	†††

*$P < 0.05$, **$P < 0.01$, ***$P < 0.001$: significantly different for OVX vehicle group
†$P < 0.05$, ††$P < 0.01$, †††$P < 0.001$: significantly different for sham group

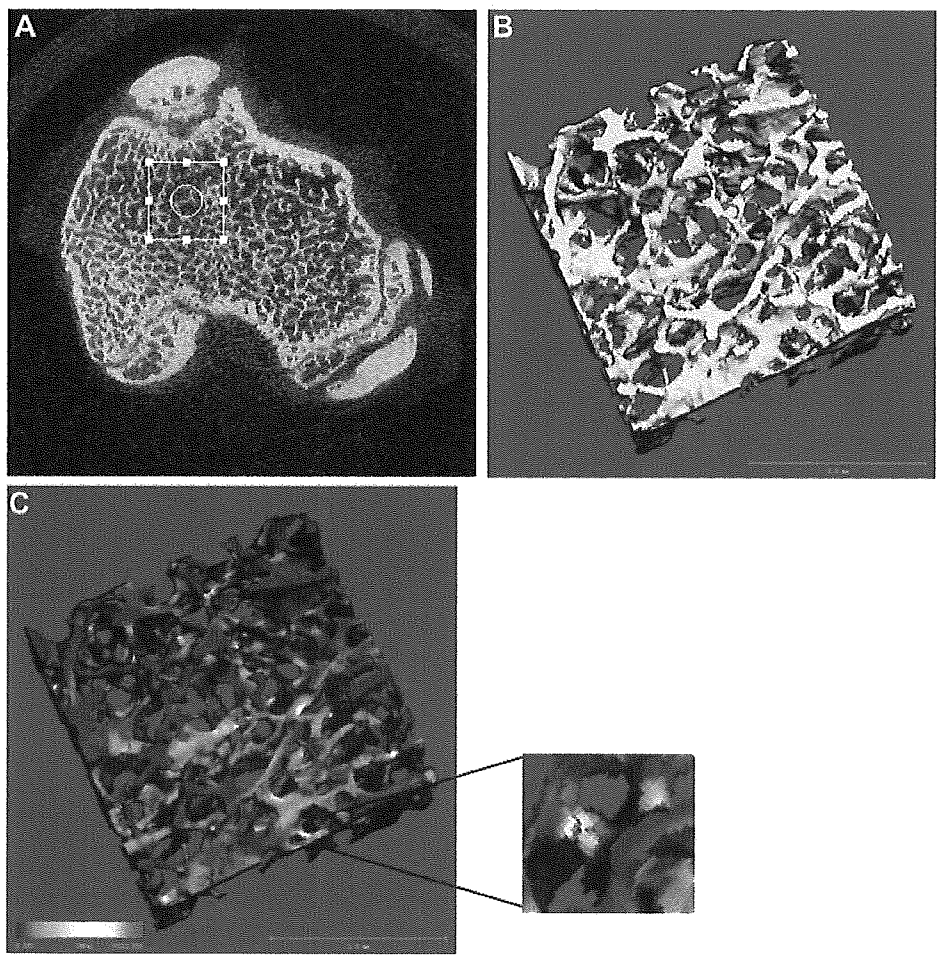

Fig. 2A–C Compression and shear simulation of three orthogonal directions. **A** The region of proximal tibia that was extracted for finite element analysis is shown. *The circle in the center* of the cubic region indicates the region that we used for calculating the degree of anisotropy. **B** The original 3D micro-CT image (upper half of the total region). **C** The 3D distribution image of von Mises stress (upper half of the total region). A high-stress region is highlighted in red in the magnified view

Table 2 Biomechanical parameters in the sham and OVX rats treated with risedronate (mechanical DA = the largest Young's modulus/the third Young's modulus, *NS* not significant)

Group	Young's modulus	*P*		Shear modulus	*P*		Mechanical DA	*P*	
Sham	1,074 ± 454			208 ± 154			6.4 ± 5.6		
OVX vehicle	361 ± 300		††	82 ± 105		NS	82.8 ± 58.5		†
OVX risedronate 0.1 mg/kg per day	527 ± 257	NS	††	72 ± 67	NS	†	74.1 ± 65.0	NS	††
OVX risedronate 0.5 mg/kg per day	638 ± 161	NS	†	93 ± 125	NS	NS	20.0 ± 24.8	**	NS
OVX risedronate 2.5 mg/kg per day	3,691 ± 1,555	***	†††	1,163 ± 682	***	†††	2.7 ± 3.3	***	NS

*$P < 0.05$, **$P < 0.01$, ***$P < 0.001$: significantly different for OVX vehicle
†$P < 0.05$, ††$P < 0.01$, †††$P < 0.001$: significantly different for sham group

Effect of risedronate on trabecular biomechanical properties

The effect of risedronate on biomechanical properties of trabecular bone was investigated by FEA, since compression testing of trabecular bone of the tibia is difficult. The microstructural parameters in the cubic bone region extracted for FEA (VOI-2) (Fig. 2) correlated highly with those in the whole trabecular bone region (VOI-1) ($P < 0.0001$ for BV/TV, connectivity density, SMI, Tb.N, Tb.Th, and Tb.Sp and $P < 0.05$ for DA). The magnitude of changes in this cubic region was greater than in the whole trabecular region for OVX as well as treatment groups (data not shown).

Table 2 shows Young's and shear moduli in the maximal principal direction in OVX rats and risedronate-treated OVX rats. OVX caused a significant decrease in Young's modulus, and tended to decrease shear modulus, compared with the sham group. Treatment with risedronate at the dose of 2.5 mg/kg significantly increased Young's and shear moduli, even above the values of the sham group. When mechanical DA was calculated as the ratio of the largest Young's modulus divided by the third Young's modulus, it was increased by OVX and was decreased by treatment with risedronate (Table 2).

Correlation between microstructural changes and biomechanical properties

Table 3 summarizes the results of multiple linear regression analysis to see how BV/TV and microstructural parameters contribute to bone strength. BV/TV correlated highly with Young's modulus in sham and risedronate groups at 0.5 mg/kg and 2.5 mg/kg ($R^2 = 0.73$–0.84). In the sham group, the addition of structural parameters did not affect Young's modulus. In contrast, in risedronate at 0.5 mg/kg and 2.5 mg/kg the correlation was increased substantially by the addition of structural parameters to BV/TV, notably SMI and connectivity density ($R^2 = 0.88$ in risedronate (RIS) 0.5 mg/kg, $R^2 = 0.93$ in RIS 2.5 mg/kg).

Discussion

Microstructural deterioration caused by estrogen deficiency is characterized by progression of localized trabecular surface resorption [7], and SMI and connectivity density are considered to be the most sensitive parameters to reveal surface contour and disconnectivity of trabeculae, respectively. In the current study we found the impact of risedronate treatment on the trabecular microstructure of OVX rat. Multiple linear regression analysis revealed a strong correlation of SMI and connectivity density with Young's modulus as well as the shear modulus. The combination of BV/TV with SMI or connectivity density explained 90% of changes in Young's modulus or shear modulus. A previous study on the effect of risedronate in calcium-deficient OVX minipigs [3] showed that BV/TV alone could explain 76% of the observed variability in bone strength and that the combination of bone volume and architectural variables accounted for >90% of mechanical strength. Although the animals used (minipig vs rat) and skeletal sites examined (vertebra vs tibia) differ, our results are consistent with those of their study.

In the sham group BV/TV alone showed high correlation with Young's modulus and shear modulus, and the addition of trabecular microstructural parameters did not increase correlation, suggesting that it is mainly bone volume that determines mechanical property under physiological conditions. In contrast, in OVX rats, neither BV/TV nor trabecular microstructural parameters showed high correlation with biomechanical properties. We observed in our previous experiments that OVX induced marked structural deterioration in the central part of spongiosa while relatively preserving the structure at the peripheral part of spongiosa close to the cortex of the tibia [18]. FEA in the present study was performed at the central part of the tibial metaphysis, where isolated, segmented structures existed in the OVX group. Thus, there may be dissociation between microstructural parameters calculated at the central region with deteriorated trabecular structure and parameters that are involved in bone strength.

Table 3 R^2 values of multiple linear regression analysis between microstructural parameters and biomechanical properties in individual groups. $R^2(BV/TV)$ the coefficient of biomechanical properties with BV/TV, $R^2(BV/TV+)$ the coefficient of biomechanical properties with BV/TV and another microstructural parameter. Values are shown when their P values were significant ($P < 0.05$)

Parameter	Sham		OVX		RIS 0.1		RIS 0.5		RIS 2.5			
Young's modulus	R^2(BV/TV) 0.85	R^2(BV/TV +)	R^2(BV/TV) 0.56*	R^2(BV/TV +)	R^2(BV/TV) 0.63	R^2(BV/TV +)	R^2(BV/TV) 0.73	R^2(BV/TV +)	R^2(BV/TV) 0.80	R^2(BV/TV +)		
						SMI 0.75		SMI 0.88		SMI 0.93		
						ConnD 0.74		ConnD 0.88		ConnD 0.93		
								Tb.N 0.84		Tb.Th 0.90		
										Tb.Sp 0.90		
										Tb.N 0.88		
Shear modulus	R^2(BV/TV) 0.85	R^2(BV/TV +)	R^2(BV/TV) 0.48*		R^2(BV/TV) 0.69	R^2(BV/TV +)	R^2(BV/TV) 0.74	R^2(BV/TV +)	R^2(BV/TV) 0.84	R^2(BV/TV +)		
						SMI 0.82		ConnD 0.90		SMI 0.99		
						ConnD 0.81		SMI 0.89		ConnD 0.98		
						Tb.Sp 0.77		Tb.N 0.82		Tb.Sp 0.92		
						Tb.N 0.75						

*The P values of R^2 were not significant ($P > 0.05$)

In risedronate-treated group, the addition of microstructural parameters to BV/TV significantly increased correlation with bone strength, suggesting that alterations in 3D structure contribute to improvements in the biomechanical property by the drug. Risedronate may have the potential to remodel trabecular structure so that it can adapt to greater mechanical stress. Treatment with risedronate decreased the mechanical DA, which was increased by OVX, suggesting that risedronate maintained the biomechanical balance in any direction.

Our results suggest that an important mechanism underlying the biomechanical efficacy of risedronate in trabecular bone is to maintain the shape of trabeculae and their connectivity. This concept is supported by a previous histomorphometric study [19] on female beagles treated with risedronate (0.1, 0.5, or 2.5 mg/kg per day orally) showing that risedronate decreased final erosion depth at doses of 0.5 and 2.5 mg/kg and reduced activation frequency at 2.5 mg/kg. Bisphosphonates bind preferentially to sites of active resorption (where bone mineral or hydroxyapatite is exposed) [20] and inhibit osteoclast-mediated bone resorption. Bisphosphonates act to prevent bone loss at resorption sites, thereby preventing localized thinning of trabeculae and deterioration of 3D microstructure.

A limitation of this study was that the effect of mineralization on bone strength was not taken into account. The micro-CT based FEA determines mechanical property on the basis of the structure, not on the change in mineralization, which is affected by treatment with bisphosphonate [21]. In the future, higher resolution 3D images such as synchrotron radiation CT will provide more accurate information on mechanical property from the aspects of both structure and mineralization.

In conclusion, our results support the concept that, in addition to increasing bone mass, risedronate improve bone biomechanical properties through alterations of trabecular structure, especially its shape and connectivity. Coupled microstructural and micro-finite element analyses provide a useful tool for us to understand the mechanism of action of anti-resorptive agents, such as risedronate, from the perspective of how micro-architecture impacts on biomechanical property.

Acknowledgements We thank Dr. Kyoji Ikeda (Department of Bone and Joint Disease, The Research Institute, National Center for Geriatrics and Gerontology) for suggestions on the manuscript. We are grateful for the assistance of Mr. Jun Kono (Department of Radiology, Nagasaki Saiseikai Hospital). This study was supported in part by the Program for Promotion of Fundamental Studies in Health Science of the Organization for Pharmaceutical Safety and Research of Japan [Masako Ito (no. MF-14)] and by grant-in-aid for scientific research from the Ministry of Education in Japan [Masako Ito (no. 13670949)].

References

1. Wasnich RD, Paul D, Miller PD (2000) Antifracture efficacy of antiresorptive agents are related to changes in bone density. J Clin Endocrinol Metab 85:231–236

2. Reginster J-Y, Minne HW, Sorensen OH, Hooper M, Roux C, Brandi ML, Lund B, Ethgen D, Pack S, Roumagnac I, Eastell R (2000) Randomized trial of the effects of risedronate on vertebral fractures in women with established postmenopausal osteoporosis. Osteoporos Int 11:83–91
3. Borah B, Dufrensne TE, Chmielewski PA, Gross GJ, Prenger MC, Phipps RJ (2002) Risedronate preserves trabecular architecture and increases bone strength in vertebra of ovariectomized minipigs as measured by three-dimensional microcomputed tomography. J Bone Miner Res 17:1139–1147
4. Parfitt AM (1992) Implications of architecture for the pathogenesis and prevention of vertebral fracture. Bone 13:S41–S47
5. Ruegsegger P, Koller B, Mueller R (1996) A microtomographic system for the non-destructive evaluation of bone architecture. Calcif Tissue Int 58:24–29
6. Mueller R, Hahn M, Vogel M, Delling G, Ruegsegger P (1996) Morphometric analysis of non-invasively assessed bone biopsies: comparison of high-resolution computed tomography and histologic sections. Bone 18:215–220
7. Ito M, Nishida A, Nakamura T, Uetani M, Hayashi K (2002) Differences of three-dimensional trabecular microstructure in osteopenic rat models caused by ovariectomy and neurectomy. Bone 30:594–598
8. Ito M, Nakamura T, Matsumoto T, Tsurusaki K, Hayashi K (1998) Analysis of trabecular microarchitecture of human iliac bone using microcomputed tomography in patients with hip arthrosis with or without vertebral fracture. Bone 23:163–169
9. Hildebrand T, Ruegsegger P (1997) A new method for the model-independent assessment of thickness in three-dimensional images. J Microsc 185:67–75
10. Laib A, Hildebrand T, Hauselmann HJ, Ruegsegger P (1997) Ridge number density: a new parameter for in vivo bone structure analysis. Bone 21:541–546
11. Hildebrand T, Ruegsegger P (1997) Quantification of bone microarchitecture with the structure model index. Comput Methods Biomech Biomed Engin 1:15–23
12. Ulrich D, van Rietbergen B, Laib A, Ruegsegger P (1999) The ability of three-dimensional structural indices to reflect mechanical aspects of trabecular bone. Bone 25:55–60
13. Boyce RW, Ebert DC, Youngs TA, Paddock CL, Mosekilde L, Stevens ML, Gundersen HJ (1995) Unbiased estimation of vertebral trabecular connectivity in calcium-restricted ovariectomized minipigs. Bone 16:637–642
14. Odgaard A, Gundersen HJ (1993) Quantification of connectivity in cancellous bone, with special emphasis on 3-D reconstructions. Bone 14:173–182
15. van Rietbergen B, Weinans H, Huiskes R, Odgaard A (1995) A new method to determine trabecular bone elastic properties and loading using micromechanical finite-element models. J Biomech 28:69–81
16. van Rietbergen B, Huiskes R, Weinans H, Odgaard A, Kabel J (1995) The role of trabecular architecture in the anisotropic mechanical properties of bone. In: Odgaard A, Weinans H (eds) Bone structure and remodeling, World Scientific, Singapore, pp 137–145
17. van Rietbergen B, Odgaard A, Kabel J, Huiskes R (1996) Direct mechanics assessment of elastic symmetries and properties of trabecular bone architecture. J Biomech 29:1653–1657
18. Ito M, Nishida A, Nakamura T, Uetani M, Hayashi K (2002) Differences of three-dimensional trabecular microstructure in osteopenic rat models caused by ovariectomy and neurectomy. Bone 30:594–598
19. Boyce RW, Paddock CL, Gleaso JR, Sletsema WK, Eriksen EF (1995) The effects of risedronate on canine cancellous bone remodeling: three-dimensional kinetic reconstruction of the remodeling site. J Bone Miner Res 10:211–221
20. Lin JH (1996) Bisphosphonates: a review of their pharmacokinetic properties. Bone 18:75–85
21. Roschger P, Rinnerthaler S, Yates J, Rodan GA, Fratzl P, Klaushofer K (2001) Alendronate increases degree and uniformity of mineralization in cancellous bone and decreases the porosity in cortical bone of osteoporotic women. Bone 29:185–191

Effects of a prostaglandin EP4 agonist, ONO-4819, and risedronate on trabecular microstructure and bone strength in mature ovariectomized rats

Masako Ito[1], Keiji Nakayama[2], Akira Konaka[2], Kiyoto Sakata[2], Kyoji Ikeda, [3] and Takayuki Maruyama[2]

[1]Department of Radiology, Nagasaki University School of Medicine, Nagasaki 852-8501 Japan

[2] Minase Research Institute, Ono Pharmaceutical Co., Ltd., Osaka, 618-8585, Japan

[3] Department of Bone and Joint Disease, The Research Institute, National Center for Geriatrics and Gerontology (NCGG), Obu, Aichi 474-8522, Japan

Corresponding author: Masako Ito, M.D., at Department of Radiology, Nagasaki University, Nagasaki 852-8501, Japan

Telephone & fax: +81-95-849-7255

e-mail: masako@net.nagasaki-u.ac.jp

Running title: EP4 agonist and risedronate

Masako Ito and Keiji Nakayama contributed equally to this work.

Abstract

The effects of a prostaglandin EP4 agonist, ONO-4819, and risedronate, a representative anti-resorptive drug, on trabecular microarchitecture and biomechanical properties were investigated in mature estrogen-deficient rats; and which affected microstructural components that contributed to the improvement of bone strength were also determined. Thirty-three-week-old OVX rats were treated with various doses of ONO-4819, risedronate or their combination for 11 weeks. Bone mineral density (BMD), trabecular microstructure, and biomechanical strength were determined at the proximal tibia by peripheral quantitative CT, micro CT, and finite element analysis, respectively. Bone histomorphometry was performed at the same site. The results of trabecular structure analysis indicated that whereas risedronate functioned mainly in maintaining trabecular connectivity, ONO-4819 converted the fragile rod-like trabeculae caused by estrogen deficiency to a plate-like structure. In addition, ONO-4819 is one of the few drugs that are capable of increasing trabecular thickness. When the 2 drugs were combined, the beneficial effects of each drug on the trabecular microarchitecture by each drug were maintained, resulting in their additive effects on bone strength. The results of bone histomorphometry suggest that ONO-4819 caused an increase in the rate of bone formation by stimulating the differentiation/recruitment of osteoblasts as well as their mineralizing function. ONO-4819 did not stimulate bone resorption, but rather exerted an anti-resorptive function within a certain dose range. ONO-4819 and risedronate increased BMD and improved trabecular structure and biomechanical strength in an additive and independent manner. Thus, EP4 agonist

ONO-4819 in combination with risedronate may be an effective treatment for osteoporosis.

Key words: prostaglandin; bone quality; microcomputed tomography

Introduction

Prostaglandins (PGs), especially those of the E series, are multifunctional regulators of bone metabolism (1). PGs are produced by osteoblasts and potently stimulate bone resorption (2). However, it has also been shown that PGE_2 stimulates new bone formation *in vivo* (3, 4). PGE_2 exerts its biological effects through interaction with specific cell-surface receptors existing as 4 subtypes, i.e., EP1, EP2, EP3, and EP4 (5). Among these receptor subtypes, EP4 and EP2, once activated, elevate the level of intracellular cAMP, which action is thought to mediate the bone resorption-stimulating effect of PGE_2 (6,7). In contrast, we earlier demonstrated by periosteal injection and callus formation assay that thickening of the femoral cortex in response to PGE_2 is abrogated specifically in mice lacking EP4 and that an EP4-specific agonist, but not other subtype agonists, mimics the stimulating effect of PGE_2 (8). These results suggest that the bone anabolic action of PGE_2 is mediated mainly through EP4, and raise the possibility that selective EP4 agonists may be applicable for the treatment of metabolic bone diseases, including osteoporosis.

In the present study, in order to gain further insight into the mechanism of action, the effects of ONO-4819, a newer compound with increased chemical stability, either alone or in combination with risedronate, on bone remodeling was studied histomorphometrically in a rat model of osteoporosis due to estrogen deficiency. In addition, the trabecular microarchitecture was assessed by micro-computed tomography, together with biomechanical properties by finite element analysis, to examine how the microstructural alterations in response to an anabolic compound, an anti-resorptive drug,

or their combination contribute to the improvement of biomechanical strength.